The solution for the cut structure is therefore [see Eq. (11a)]

$$\bar{F}(M) = f(M,H)P(H) + f(M,J)R(J)$$

$$\begin{bmatrix}\bar{F}(4)\\ \bar{F}(5)\\ \bar{F}(6)\\ \bar{F}(7)\\ \bar{F}(8)\\ \bar{F}(9)\end{bmatrix} = \begin{bmatrix}-1/4\\ L/8\\ -1/4\\ L/8\\ -1/4\\ -L/8\end{bmatrix}[P_1] + \begin{bmatrix}-1/4 & 0\\ L/8 & 0\\ -1/4 & -3/4L\\ L/8 & 1/4\\ -1/4 & 0\\ -L/8 & 0\end{bmatrix} \times \begin{bmatrix}7\\ -4L\end{bmatrix}[P_1/9] = \begin{bmatrix}-4\\ 2L\\ -1\\ L\\ -4\\ -2L\end{bmatrix}[P_1/9]$$

and [see Eq. (12a)]

$$D(M) = \delta(M,H)P(H) + \delta(M,J)R(J)$$

$$\begin{bmatrix}\Delta_1\\ \theta_2\end{bmatrix} = \begin{bmatrix}48EI/L^3 & 0\\ 0 & 8EI/L\end{bmatrix}^{-1}\begin{bmatrix}P_1 + 7P_1/9\\ 0 - 4P_1L/9\end{bmatrix} = \begin{bmatrix}P_1L^2/24EI\\ -P_1L^2/18EI\end{bmatrix}$$

The analysis of the cut structure as an original structure would result in

$$\begin{bmatrix}\Delta_1\\ \theta_2\end{bmatrix} = \begin{bmatrix}36EI/L^3 & 6EI/L^2\\ +\ 6EI/L^2 & 4EI/L\end{bmatrix}^{-1}\begin{bmatrix}P_1\\ 0\end{bmatrix}$$

with identical displacements and internal loads.

Equations (11, 12, and 14) represents a relatively simple procedure to obtain the structural behavior of a damaged structure. The equations can be applied with or without the assistance of digital computing machines and permit the analyst to visualize how the loads and deformations will change when the structure suffers a local failure, yielding, or instability. This can be very valuable in obtaining efficient designs since the designer can readily grasp how the loads will be redistributed when a local member is not adequate and thereby obtain a better proportioned structure. In addition, a more realistic ultimate strength capacity of the structure based upon limit rather than elastic analysis can be utilized.

Determination of the Wake behind a Bluff Body of Revolution at High Reynolds Numbers

JEAN-YVES PARLANGE*
Yale University, New Haven, Conn.

1. Introduction

THE properties of the laminar wake formed by a bluff body in its steady motion through an incompressible fluid at high Reynolds number are not completely understood at present. Most of the existing theories have been primarily concerned with the two-dimensional case.[1-4] Although we are interested in the axisymmetric case, it is worthwhile to review the difficulties encountered in two dimensions.

The freestream solution due to Kirchhoff cannot describe a (complete) two-dimensional wake since it violates the intuitive result that the disturbance must die down at infinity downstream.[1] Batchelor[1] proposed a model with circulation in a finite wake. There are some experimental evidences[2] that, for a two-dimensional wake, the drag coefficient approaches a finite limit as the Reynolds number Re approaches infinity. Kirchhoff's model predicts a finite drag coefficient while Batchelor's model on the contrary leads to a zero drag coefficient as $Re \to \infty$. Recently Roshko[3] and Sychyev[4] have developed, independently, similar theories giving both a finite drag coefficient as $Re \to \infty$ and a finite wake for $Re \gg 1$. We shall see that the difficulty with Batchelor's model in two dimensions, which indeed makes it suspect, does not arise in the axisymmetric case. Batchelor has proven[5] that for a recirculating two-dimensional flow the vorticity ξ is constant in the cavity except possibly in thin boundary layers. The circulation in the cavity is induced by contact with the "outside," which could be for instance a rotating container or another flow (like in the case of a wake). If the outside tends to make the flow rotate in only one direction, no ambiguity arises about the response of the fluid in the cavity.† On the contrary, for a two-dimensional wake the flows on each side of the wake (the outside) tend to make the wake circulate in opposite direction. Consequently, the response of the wake is not obvious. Part of the wake may remain essentially stagnant (the near wake of Roshko and Sychyev), or the wake may be composed of two cells with circulation in opposite directions. Each of the two cells then separately obey Batchelor's theorem of constant vorticity (but with opposite signs in each cell).

For an axisymmetric flow experimental‡ and numerical[8] evidence indicates that no part of the fluid in the wake is stagnant. A superficial look at Fig. 1 might still give the impression that the outside flows on opposite sides of the wake work at cross purposes, hence raising doubts once more about the response of the fluid in the cavity. Actually the two apparent cells in Fig. 1 belong to the same continuous cell because of the axisymmetry of the flow. The vorticity does not change sign but is in the same azimuthal direction at each point. Then, if y is the distance from any point to the axis, Batchelor's theorem[5,7] indicates that ξ/y is uniform at each point in the wake (excepting thin boundary layers). In conclusion for the axisymmetric case the outside pulls consistently all around the wake and tends to make the fluid circulate in only one possible way; hence, there is no doubt that we have a completely circulating wake, obeying Batchelor's theorem.[5,7]

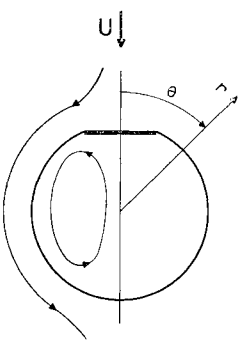

Fig. 1 Sketch of wake and streamlines.

Received June 12, 1969. The author acknowledges a helpful discussion with Y. Rimon of the Applied Mathematics Laboratory, Washington, D. C. and valuable correspondence with A. Roshko of the California Institute of Technology.

* Associate Professor of Engineering and Applied Science.

† One has only to think about the fluid in a circular cylinder rotating at uniform angular velocity. Once a steady state is reached, the fluid rotates at the same angular velocity (uniform vorticity).

‡ For instance in the case of spherical cap bubbles,[6] the circulation in the wake can be visualized very easily with small air bubbles. For the related problem of water bells[7] (the water sheets are the outside) the circulation is clearly seen by injection of smoke. In both cases the assumption that Batchelor's theorem for axisymmetric flow[5] holds in the whole cavity leads to results[6,7] well checked experimentally.

2. Asymptotic Solution for the Axisymmetric Wake

We are interested in the limiting case of a very large Reynolds number, $Re \gg 1$, so that viscous effects are negligible§ as a first approximation. We define the Reynolds number by

$$Re = UD/\nu \tag{1}$$

where U is the steady velocity of the bluff body, ν the kinematic viscosity, and D the diameter of the body's largest cross section. We assume that the bluff body's length is either of order D (spherelike) or much smaller than D (disklike). The reasoning does not apply to very slender, needlelike, bodies. It is quite intuitive that for increasing Re the wake increases in size. If a is a characteristic dimension of the wake, we shall see later that $D/a \to 0$ as $Re \to \infty$. Consequently, we commit only a negligible error if, in the first approximation, we disregard the body entirely for the determination of the streamlines. This approximation is obviously incorrect near the body. The details of the flow have to be determined near the body to compute the drag F. One can say that the role of the body is primarily to provide the energy FU necessary to maintain the flow against the viscous dissipation $\bar{\Phi}$, with

$$FU = \bar{\Phi} \tag{2}$$

Except near the body, the flow can be determined easily using Batchelor's theorem. The same equations have been solved before in a different case.[6] It is found, calling ψ the stream function and using spherical polar coordinates (see Fig. 1),

$$\psi = 3Ur^2 \sin^2\theta(r^2 - a^2)/4 \tag{3}$$

inside the wake

$$\psi = \tfrac{1}{2}Ur^2 \sin^2\theta(1 - a^3/r^3) \tag{4}$$

outside the wake

The stream functions are written for a motionless body, the fluid having the velocity U at infinity, rather than for a body moving in a fluid at rest. The equations indicate that for $Re \gg 1$ the wake is a sphere of radius a. The velocity U being given, the flow is entirely determined (except near the body) once a is known. The viscous dissipation is[6]

$$\bar{\Phi} = 30\ \pi\nu a\rho U^2 \tag{5}$$

where ρ is the density. If we can evaluate F, then Eq. (2) provides the additional equation necessary to compute a. Clearly, the value of F depends on the exact shape of the body. For instance, consider the case of a thin disk (Fig. 1). Since $D/a \ll 1$, it is quite intuitive that the pressure p acting on the disk can be determined from the potential flow over the sphere of radius a [Eq. (4)]. On the other hand, the back pressure below the disk should be fairly uniform since it is a stagnation region where the flow changes direction drastically (at the difference of the outside where the flow is much smoother). Actually, this rather simplistic argument is checked very well from numerical computations for Reynolds numbers as low as 300 (see Ref. 8, Fig. 12). Over the disk then (since the viscous stress is negligible for $Re \gg 1$),

$$dp = \rho u\, du \tag{6}$$

where, from (4),

$$u \simeq \tfrac{3}{2}U\theta \tag{7}$$

§ We must remember of course that, even for $Re \gg 1$, viscosity is of fundamental importance in the problem as it is responsible for the diffusion of vorticity and the validity of Batchelor's theorem.

p_0 being the back pressure, we obtain

$$F = \int_0^{D/2a} 2\pi a^2\theta(p_0 - p)d\theta \tag{8}$$

where, from (6) and (7),

$$p - p_0 = 9U^2\rho[\theta^2 - D^2/4a^2]/8 \tag{9}$$

Consequently,

$$F = 9\pi U^2\rho D^4/2^8a^2 \tag{10}$$

and, from (2) and (5),

$$D/2a = (320/3\ Re)^{1/3} \tag{11}$$

Equation (11) gives a and completes the determination of the flow. Notice that indeed $D/2a \to 0$ as $Re \to \infty$, but the limit is reached very slowly because of the $\frac{1}{3}$ power and also because of the relatively large coefficient. The drag coefficient is defined by $C_D = 8F/\rho U^2\pi D^2$ or

$$C_D = 2(45/Re)^{2/3} \tag{12}$$

As expected $C_D \to 0$ as $Re \to \infty$.

3. Conclusion

A very large Reynolds number is necessary for the theory to be valid. This introduces experimental difficulties since the flow may become unstable and turbulent. Fortunately, numerical solutions can be obtained which are constrained to give a steady laminar flow no matter how large the Reynolds number is.[8] It is interesting to compare some of the results. For instance, from Fig. 5 of Ref. 8, it is clear that for $Re = 600$ the wake is already spherical. Also, for $Re = 600$, Eq. (11) gives $2a/D = 1.8$ (this is not very large since Re is only moderately high), which is almost exactly the value one obtains from Fig. 5.[8]

Clearly, if the body is not a disk (and not needlelike) the wake remains spherical and the dependence of a and C_D on the Reynolds numbers remains unchanged (even if the exact numerical coefficients will depend on the exact shape of the body). Consequently, for a reasonable axisymmetric bluff body and a steady laminar flow we have

$$D/2a \sim Re^{-1/3},\ C_D \sim Re^{-2/3} \tag{13}$$

Finally, notice that the tangential viscous stresses deduced from (3) and (4) are not continuous at the sphere. Consequently, stress-induced boundary layers develop along the sphere. Determination of these boundary layers leads to small corrections (or order $Re^{-1/2}$) in our previous results. The same technique which has been used previously[9] for drops could be applied here.

References

[1] Batchelor, G. K., "A Proposal Concerning Laminar Wakes behind Bluff Bodies at Large Reynolds Number," *Journal of Fluid Mechanics*, Vol. 1, Pt. 4, Oct. 1956, pp. 388–398.

[2] Acrivos, A. et al., "The Steady Separated Flow past a Circular Cylinder at Large Reynolds Numbers," *Journal of Fluid Mechanics*, Vol. 21, Pt. 4, April 1965, pp. 737–760.

[3] Roshko, A., "A Review of Concepts in Separated Flow," *Proceedings of the Canadian Congress of Applied Mechanics*, Vol. 3, May 1967, pp. 81–115.

[4] Sychyev, V. V., "On Steady Laminar Flow of a Fluid Around a Bluff Body at Large Reynolds Numbers," *8th Symposium on Mechanics of Fluids*, transl. by R. P. Simha, National Aeronautical Laboratory, Bangalore, India, Feb. 1969.

[5] Batchelor, G. K., "On Steady Laminar Flow with Closed Streamlines at Large Reynolds Number," *Journal of Fluid Mechanics*, Vol. 1, Pt. 2, July 1956, pp. 177–190.

[6] Parlange, J.-Y., "Spherical Cap Bubbles with Laminar Wakes," *Journal of Fluid Mechanics*, Vol. 37, Pt. 1, June 1969, pp. 257–264.

[7] Parlange, J.-Y., "A Theory of Water-Bells," *Journal of Fluid Mechanics*, Vol. 29, Pt. 2, Aug. 1967, pp. 361–372.

[8] Rimon, Y., "Numerical Solution of the Incompressible Time Dependent Viscous Flow past a Thin Oblate Spheroid," TN AML-24-68, July 1968, Applied Mathematics Laboratory, Washington, D. C., to be published in *The Physics of Fluids*.

[9] Parlange, J.-Y., "Motion of Spherical Drops at Large Reynolds Numbers," *Acta Mechanica*, 1969, to be published.

Estimation of Aerodynamic Center and Span Load Distributions of Swept Wings

D. P. Hickey*
Douglas Aircraft Company, Long Beach, Calif.

Nomenclature

a or a_ν = local sectional lift curve slope
AR = aspect ratio
b = wing span
$b_{\nu n}$ = coefficient defined by Eq. (17) of Ref. (9)
c or c_ν = local wing chord, bar denotes average chord
M = Mach number
m = total number of spanwise control stations
n = exponent defined by Eq. (6)
n_0 = exponent defined by Eq. (5)
R = Reynolds number based on mean aerodynamic chord
x_{ac} = aerodynamic center position measured from wing leading edge
y_c or y_t = spanwise coordinate measured relative to wing center or tip, respectively, in terms of local chord
α or α_ν = local geometric angle of attack
γ = nondimensional circulation
η = nondimensional spanwise coordinate
λ = taper ratio
$\lambda(y)$ = parameter defined by Eqs. (1) and (2)
ν = index denoting spanwise location
$\varphi_{c/2}$ = semichord sweep angle
φ_e = effective semichord sweep angle
ω = downwash factor of wing

Introduction

THERE exist several methods for calculating the aerodynamic center distributions on swept wings. It is the purpose of this Note to indicate the most appropriate method, or methods, applicable to swept, moderate aspect ratio wings. Reference 1 presents a method which is given in two forms for determining the aerodynamic center distribution with respect to the quarterchord line of a wing. One form is the tangent approximation and the other form is the hyperbolic approximation. Reference 2 presents a method, based on the Multhopp lifting surface theory of Ref. 3, which includes a correction for wing thickness.

Discussion

The hyperbolic and tangent approximations are given in Ref. 1, as respectively.

$$\lambda(y) = \left[1 + \left(2\pi \frac{\tan\varphi_e}{\varphi_e} y\right)^2\right]^{1/2} - 2\pi \frac{\tan\varphi_e}{\varphi_e} y \qquad (1)$$

and

$$\lambda(y) = 1.40 + 1.33y - (0.16 + 7.30y)^{1/2} \qquad (2)$$

The constants in the Eq. (2) were determined such that the spanwise aerodynamic center position is tangent to the $c/4$-line [i.e., $\lambda(y) = 0$] for y equal to unity.

Received August 14, 1969.
* Senior Engineer Scientist, Aero Design Group, Aerodynamics Section. Member AIAA.

Both experimental and theoretical aerodynamic center locations are shown in Figs. 1a, 1b, 1c, and 1d for the wings of Refs. 4, 5, 6, and 7, respectively. These wings are labeled as planforms A, B, C, and D in the subsequent discussion. The geometrical characteristics of the wings are tabulated as follows:

Table 1 Geometrical characteristics of wings

Wing	AR	$\varphi_c/4$, deg	λ	Airfoil section	t/c, %
A	2.828	49.51	0.333	RAE 102	6
B	3.0	45.0	0.5	NACA 64A010	10
C	5.0	45.0	1.0	RAE 101	12
D	8.0	45.0	0.45	NACA 63A012	12

The Multhopp lifting surface theory result obtained for each wing, from a computer program based on Ref. 8, is also included for comparison. The number of control points used in the computer program was 4 chordwise and 31 spanwise (tip to tip). The experimental data shown in Fig. 1 are determined from an average of the experimental values between the angles of attack of 2° and 5°. Examination of Fig. 1 shows that the tangent approximation of Ref. 1 gives a good representation of the aerodynamic center location for all wings except the high aspect ratio wing D. In this case, either the Multhopp lifting surface theory[8] or Transonic Data Memorandum method,[2] without the thickness correction, gives good agreement with experiment. It appears from the experimental results shown in Figs. 1a, 1b, and 1d that the aerodynamic center positions do in fact follow the predicted variation in moving toward the trailing edge at the wing root and toward the leading edge at the tip. Also shown in Fig. 1c is the extended tangent, as recommended in Ref. 2, for representing the aerodynamic center distribution on the outboard portion of the wing.

One question of immediate interest is the significance of the aerodynamic center position on the loading of swept wings using the method suggested by Kuchemann.[1] This method determines the two-dimensional sectional lift curve slope for swept or unswept wings and then calculates the span loading using a quasi-lifting line analysis. The sectional lift slope is given in Ref. 1 as

$$a = a_0 \frac{\cos\varphi_e}{\sin\pi n_0} \frac{2n}{1 - \pi n(\cot\pi n - \cot\pi n_0)} \qquad (3)$$

$$\varphi_e = \varphi_{c/2}/[1 + (a_0 \cos\varphi_{c/2}/\pi A)^2]^{1/4} \qquad (4)$$

$$n_0 = \tfrac{1}{2}[1 - (\varphi_e/\pi/2)] \qquad (5)$$

and

$$n = 1 - \frac{1 + \lambda(y)(\varphi_e/\pi/2)}{2[1 + (a_0 \cos\varphi_e)/\pi A)^2]^{1/4[1+|\varphi_e|/(\pi/2)]}} \qquad (6)$$

The term $\lambda(y)$ is related to the aerodynamic center location by the expression

$$\lambda(y) = 2\pi(x_{ac} - 0.25)/\varphi_e \qquad (7)$$

The integral equation for the spanwise loading is given as

$$\frac{2b}{a(\eta)c(\eta)} \gamma(\eta) = \alpha(\eta) - \frac{\omega}{2\pi} \int_{-1}^{1} \frac{d\gamma(\eta')}{d\eta'} \frac{d\eta'}{\eta - \eta'} \qquad (8)$$

This equation can be solved by the Multhopp integration method[9] which results in the system of linear equations

$$\gamma_\nu \left(b_{\nu\nu} + \frac{2b}{\omega a_\nu c_\nu}\right) = \frac{\alpha_\nu}{\omega} + \sum_{n=1}^{m}{}' b_{\nu n}\gamma_n \qquad (9)$$